nature astronomy

SUPPLEMENTARY INFORMATION
https://doi.org/10.1038/s41550-018-0426-z

In the format provided by the authors and unedited.

The detection of the imprint of filaments on cosmic microwave background lensing

Siyu He[1,2,3*], Shadab Alam[4,5], Simone Ferraro[6,7], Yen-Chi Chen[8] and Shirley Ho[1,2,3,6]

[1]Carnegie Mellon University, 5000 Forbes Avenue, Pittsburgh, PA, USA. [2]McWilliams Center for Cosmology, Carnegie Mellon University, Pittsburgh, PA, USA. [3]Lawrence Berkeley National Laboratory, Berkeley, CA, USA. [4]Institute for Astronomy, University of Edinburgh, Edinburgh, UK. [5]Royal Observatory, Blackford Hill, Edinburgh, UK. [6]Berkeley Center for Cosmological Physics, University of California, Berkeley, CA, USA. [7]Miller Institute for Basic Research in Science, University of California, Berkeley, CA, USA. [8]Department of Statistics, University of Washington, Seattle, WA, USA.
*e-mail: siyuh@andrew.cmu.edu

The detection of the imprint of filaments on Cosmic Microwave Background (CMB) lensing (Supplementary information)

Siyu He[1,2,3], Shadab Alam[4,5], Simone Ferraro[6,7], Yen-Chi Chen[8], and Shirley Ho[1,2,3,6]

[1]Carnegie Mellon University, 5000 Forbes Avenue, Pittsburgh PA 15213, USA
[2]McWilliams Center for Cosmology, Carnegie Mellon University, Pittsburgh, PA 15213, USA
[3]Lawrence Berkeley National Lab, Berkeley, CA 94720, USA
[4]Institute for Astronomy, University of Edinburgh
[5]Royal Observatory, Blackford Hill, Edinburgh, EH9 3HJ , UK
[6]Berkeley Center for Cosmological Physics, University of California, Berkeley CA 94720, USA
[7]Miller Institute for Basic Research in Science, University of California, Berkeley CA 94720, USA
[8]Department of Statistics, University of Washington, Seattle, WA 98195, USA

1 Jackknife regions

To select the jackknife regions, we divide the observed sky in rectangular jackknife regions such that each region has same effective observed area by demanding equal number of randoms. We also tried to make a choice to keep the regions as close to square as possible so we don't introduce extra scales. We found that 11 × 7 (RA,DEC) jackknife regions satisfy all the constraints. We show an illustration of jackknife regions in Supplementary Figure 2.

2 Error calculation for $C_l^{\kappa f}$ from simulation

$C_l^{\kappa f}$ and C_l^{mf} are derived as

$$C_l^{\kappa f} = \frac{3H_0^2\Omega_{m,0}}{2c^2}\int_{z_1}^{z_2} dz W(z) f(z)\chi^{-2}(z)(1+z) \times P_{mf}\left(\frac{l}{\chi(z)}, z\right) \tag{1}$$

$$C_l^{mf} = \int_{z_1}^{z_2} dz \frac{H(z)}{c} f(z)\chi^{-2}(z) P_{mf}\left(\frac{l}{\chi(z)}, z\right) \tag{2}$$

By removing the appropriate functions from the integrands, which are slowly varying compared to $f(z)$, the correct expression between $C_l^{\kappa f}$ and C_l^{mf} is

$$C_l^{\kappa f} = \frac{3H_0^2\Omega_{m,0}W(z)(1+z)}{2cH(z)} C_l^{mf}$$

However, the approximations required to produce this expression are not perfect, causing the estimation of $C_l^{\kappa f}$ from simulation to slightly deviate from the true value of $C_l^{\kappa f}$. We estimate the deviation Γ by relating the theoretical prediction for $C_l^{\kappa f}$ and C_l^{mf} by the following equation

$$\Gamma = \frac{2cH(z)C_l^{\kappa f}}{3H_0^2\Omega_{m,0}W(z)(1+z)C_l^{mf}} \tag{3}$$

The result is shown in Supplementary Figure 1. We see that the Γ is less than 5% from unity, which is much smaller than $\Delta(C_l^{\kappa f})/C_l^{\kappa f}$, where $\Delta(C_l^{\kappa f})$ is the error for $C_l^{\kappa f}$. Thus, the approximation for converting C_l^{mf} to $C_l^{\kappa f}$ only causes a negligible bias.

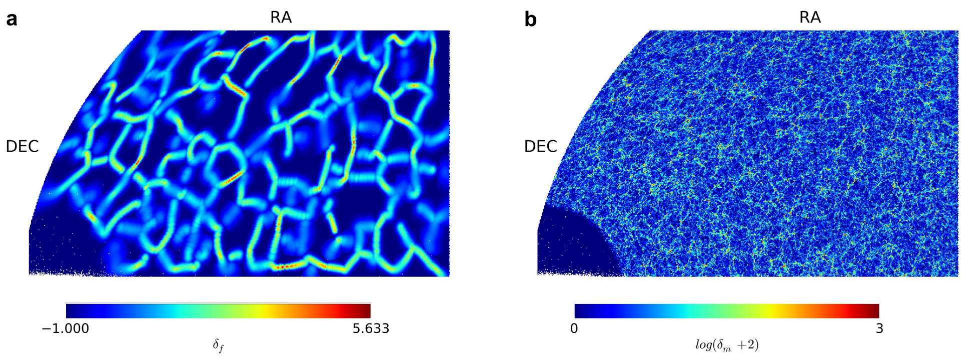

Supplementary Figure 1: A demonstration of filament intensity overdensity and corresponding dark matter particle overdensity in simulation at redshift 0.57. (***a***) filament intensity overdensity at redshift 0.57. (***b***) dark matter overdensity at redshift 0.57. The color bars show the amplitude of the overdensity field in linear scale.

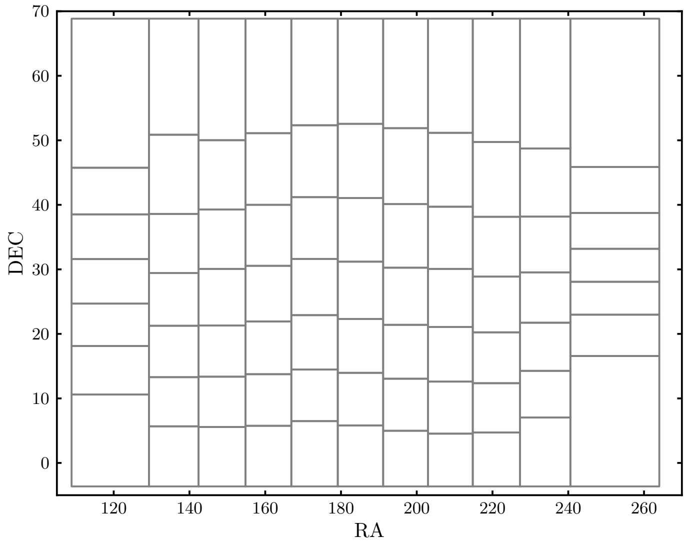

Supplementary Figure 2: Visualization of jackknife regions. The jackknife regions are chosen so that each region has same effective observed area and is close to square.

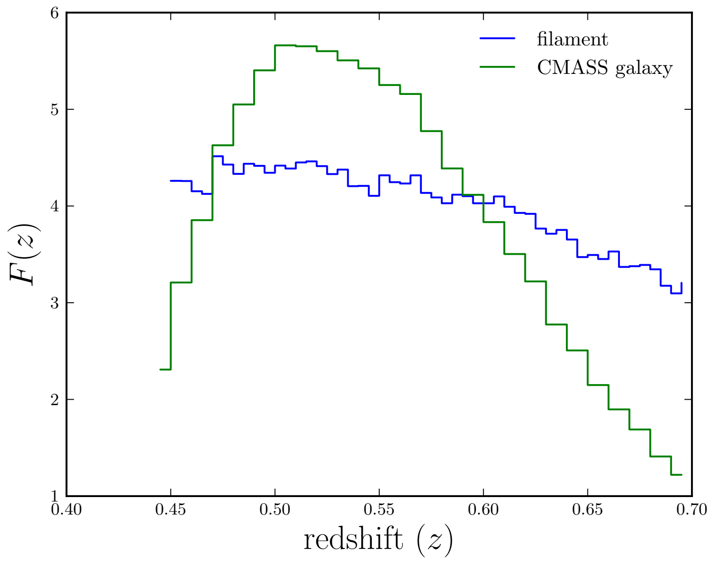

Supplementary Figure 3: Filament intensity distribution and galaxy redshift distribution as a function of redshift. The blue curve shows the filament intensity distribution as a function of redshift. The green curve shows the CMASS galaxy redshift distribution, defined as the normalized distribution of the number density of galaxies as a function of redshift. The decrease of the filament intensity distribution results from the decrease of CMASS galaxy redshift distribution, from where the filaments in each redshift slice are detected.

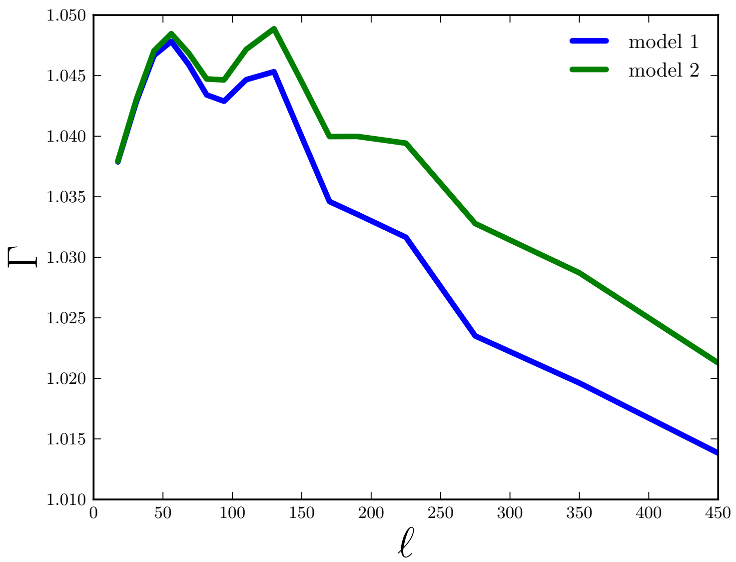

Supplementary Figure 4: Quantification of the deviation between $C_l^{\kappa f}$ estimated from simulation and from theoretical $C_l^{\kappa f}$. Since the approximations to get $C_l^{\kappa f}$ from simulations are not perfect, the $C_l^{\kappa f}$ from simulation will slightly deviate from the true value of $C_l^{\kappa f}$. Γ quantifies the deviation. In theory, We use two models for the smoothing introduced by filaments. In model1, filament length is the overall smoothing scale. In model2, filament length is the smoothing scale along the filament and we fit α for the smoothing in the perpendicular direction, where $1/k_\perp(z) \sim \alpha \times 1/k_\parallel(z)$ and k is the wavenumber in Fourier space. As shown in the plot, the deviation of $C_l^{\kappa f}$ between simulation and theory is less than 5% from unity for both theoretical models.

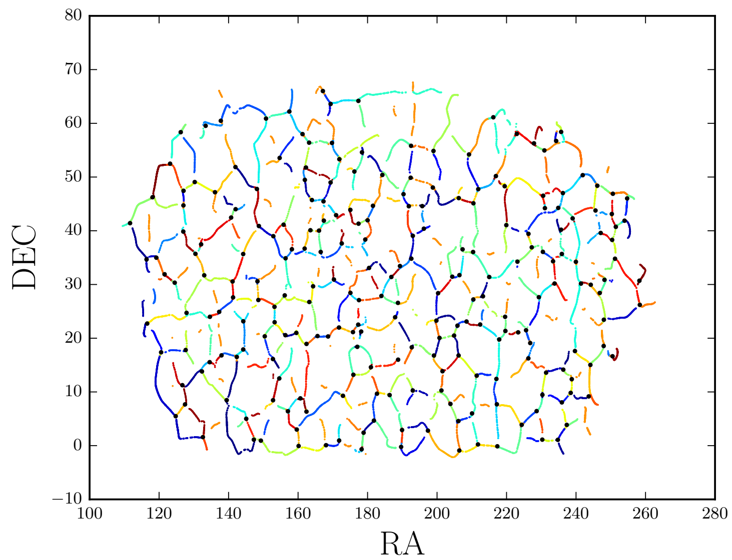

Supplementary Figure 5: Example of filament grouped in redshift bin 0.55. A line with the same color is considered as belonging to the same filament.